

# **Real-Time Observation of the Diffusion Mechanism Progression from Liquid to Solid-State of Transition Metal Complexes**

Tea-Yon Kim, Yujue Wang, Austin L. Raithel and Thomas W. Hamann\*

Department of Chemistry, Michigan State University, East Lansing, Michigan 48824-1322, United States.

\* Corresponding author

E-mail addresses: hamann@chemistry.msu.edu.

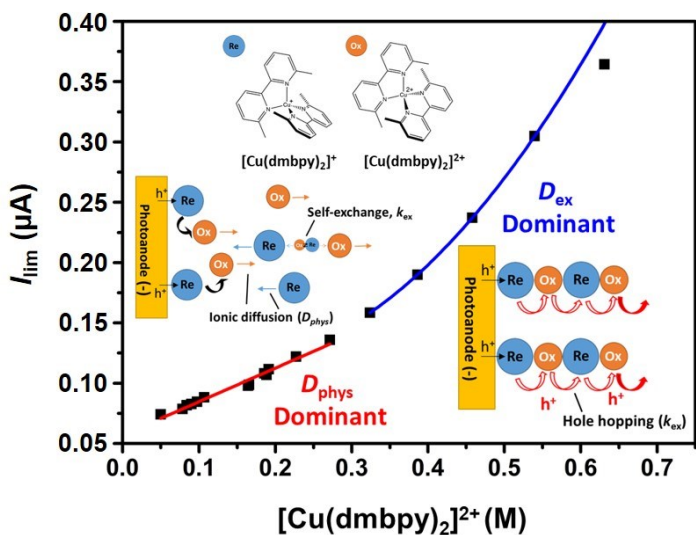
## **Keywords**

Charge transport mechanism, Transition metal complexes, Solid-state electrochemical analyses, Self-exchange reaction, Mesoscopic solar cells

## ABSTRACT

Copper complexes have recently shown remarkable performance upon conversion from liquid-based to solid-state hole transport materials (HTMs) in mesoscopic solar cells, however the diffusion mechanism is not clear. In this work we apply an *in-situ* solidification analysis of the charge diffusion and find that the dominant mechanism of  $[\text{Cu}(\text{dmbpy})_2]^{2+/+}$  (dmbpy = 6,6'-dimethyl-2,2'-bipyridine) changes from ionic to electronic diffusion. Through use of the modified Dahms-Luff equation, a fast self-exchange rate constant of hole-hopping in the HTM of  $8.3 \times 10^8$  ( $\pm 5 \times 10^7$ )  $\text{M}^{-1}\text{s}^{-1}$  is calculated, which indicates a small reorganization energy of 0.47 eV. These results introduce a new methodology to analyze the transport mechanism of solids, reveal the mechanism of charge transport in molecular-based HTMs, and offer insight into ways to control the flow of charge in optoelectronic systems.

## TOC GRAPHIC



Mechanisms of diffusion in charge transport materials (CTMs) used in modern optoelectronic applications are studied to understand their fundamental properties and improve performance.<sup>1</sup> Knowledge of the diffusion mechanism of CTMs can improve the energetic and kinetic properties, for example in mesoscopic solar cells, by controlling the conductivity in the CTM as well as the interfacial properties between the electrode and CTM.<sup>2-4</sup> The CTMs can generally be classified into two types depending on the diffusion-dominated transport mechanism: liquid electrolytes (LEs) with physical ionic diffusion governed by ion movement and solid-state hole transport materials (HTMs) with electronic diffusion by hopping.<sup>5</sup> In dye-sensitized solar cells (DSCs), even though the liquid-junction DSCs with LEs still show the highest performance ( $\sim 14.3\%$ ),<sup>6</sup> solid-state DSCs using HTM have been studied to overcome solvent leakage and evaporation which may result in poor long-term stability and limit commercialization.<sup>7</sup> As a result, solid-state DSCs have shown significantly improved device efficiency in recent years ( $\sim 11.7\%$ ).<sup>8</sup> This has been attributed to the fact that HTMs can have a faster regeneration rate and hole conductivity than LEs, but the recombination rate is also faster at the interface with the photoanode.<sup>2, 5, 8</sup> Many attempts have been made to overcome the performance drawbacks of HTMs such as improving their low hole conductivity and interfacial contact resistance.<sup>4</sup>

Copper complex HTMs were first reported as “Zombie cells” and have attracted much attention lately due to their performance exceeding that of LEs composed of the same materials.<sup>9-11</sup> Zombie cells were discovered serendipitously and have a unique manufacturing process compared to typical HTMs as a result. The organic solvent is simply evaporated from DSCs containing copper complexes in LEs.<sup>9</sup> Although these HTMs exhibit higher film conductivity and enhanced device performance from the favorable interfacial charge transfer kinetics,<sup>8-9</sup> it has only been speculated that the mechanism of hole transport within the HTM could be hopping.<sup>12</sup> On the other hand, when

HTMs were developed using cobalt and iron complexes, the device exhibited significantly lower performance than conventional HTMs employed, such as LEs and spiro-OMeTAD, in spite of their higher conductivity.<sup>13-14</sup> These results require investigation into the transport mechanism that can explain the properties of both the diffusion of CTMs and the interfacial charge transfer between the CTMs and electrodes. The self-exchange electron-transfer rate constant, which offers insight into the kinetic properties of the transition metal coordination complexes, can be used as a key parameter to understand the charge transport mechanism in general.

In this work we set out to elucidate the mechanism of charge transport with  $[\text{Cu}(\text{dmbpy})_2]^{2+/+}$  (dmbpy = 6,6'-dimethyl-2,2'-bipyridine, **Figure 1a**) upon the transition from LE to solid phase of HTM through an *in-situ* solidification analysis with an ultramicroelectrode (UME, **Figure 1b**), using the modified Dahms-Ruff equation. From the measurements of the diffusion limit current ( $I_{\text{lim}}$ ) and determination of the apparent diffusion coefficient ( $D_{\text{app}}$ ), we observe different regimes of behavior which we assign to ionic and electronic diffusion mechanisms upon solidification. These results further allow for the calculation the charge transfer self-exchange rate constant ( $k_{\text{ex}}$ ) and reorganization energy of the HTM.

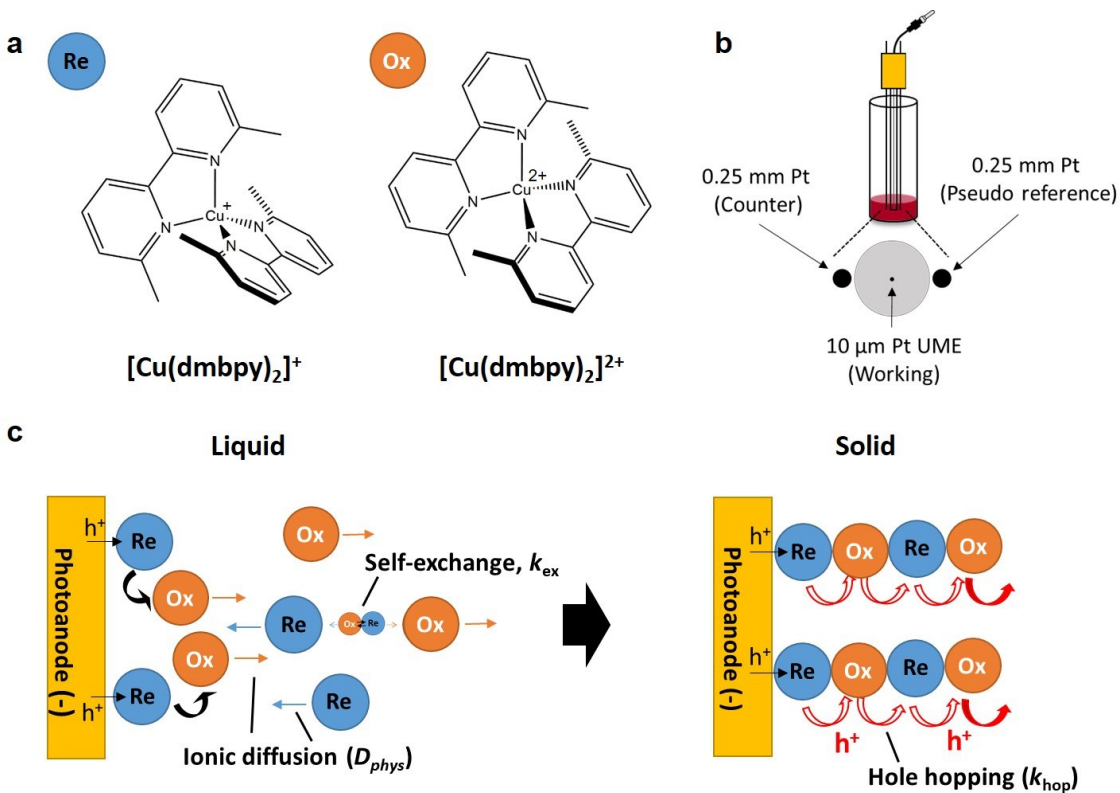


**Figure 1.** (a) Chemical structures of the redox shuttle used for this work:  $[\text{Cu}(\text{dmbpy})_2]\text{OTf}$  (Re) and  $[\text{Cu}(\text{dmbpy})_2]\text{OTf}_2$  (Ox). (b) Schematic illustration of the electrochemical cell comprised of a 10  $\mu\text{m}$  Pt disk UME for the working electrode and 0.25 mm Pt wires for the pseudo reference and counter electrode. (c) Depiction of predicted schemes of electron (hole) transport mechanism differences between the LE and HTM.

A sandwich cell configuration was initially employed to determine the diffusion mechanism(s) of  $[\text{Cu}(\text{dmbpy})_2]^{2+/+}$  during the transition from the LE to HTM using the solvent evaporation method. The  $I$ - $V$  characteristics shown in figure 2a were used to calculate the conductivities for the LE in the initial (no evaporation) condition as well as the dried HTM. In agreement with a previous report,<sup>10</sup> the HTM ( $4.77 \times 10^{-4} \text{ S cm}^{-1}$ ) exhibits a higher conductivity than the LE ( $2.58 \times 10^{-4} \text{ S cm}^{-1}$ ). In general, the conductivity of the electrolyte is related to the diffusion coefficient of the ions constituting the electrolyte.<sup>15</sup> Therefore, through the calculated conductivities above, we can indirectly predict the differences in the diffusion coefficient of copper complexes included in LE and HTM, respectively.

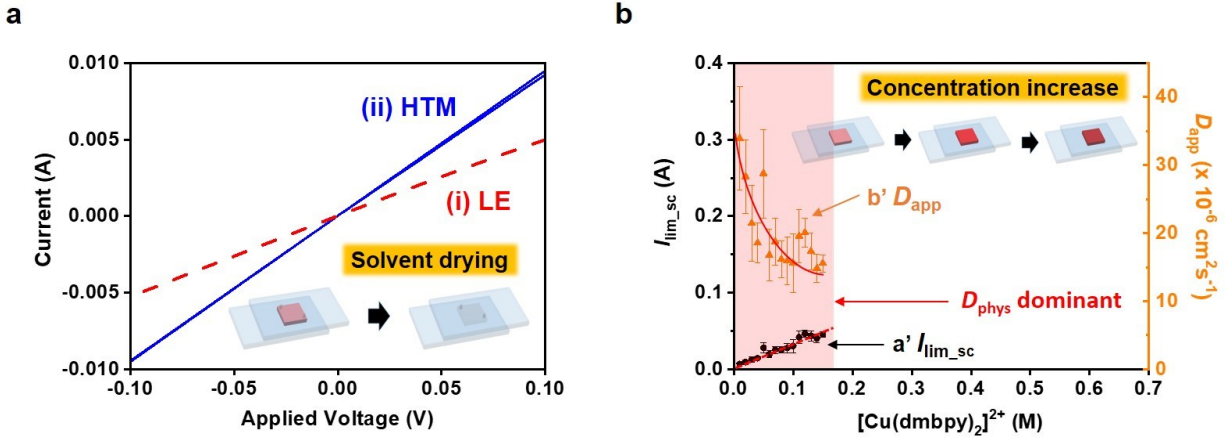


**Figure 2.** Plots of the electrochemical analysis using the sandwich configuration cells. (a) The  $I$ - $V$  characteristics to calculate the conductivities of (i) the LE (red dashed-line) and (ii) HTM (blue solid-line). The LE is composed of 0.2 M  $[\text{Cu}(\text{dmbpy})_2]^+$  and 0.05 M  $[\text{Cu}(\text{dmbpy})_2]^{2+}$  in ACN and the HTM was produced by evaporating the solvent of LE. (b) The average diffusion-limited current and correlated apparent diffusion coefficient by the sandwich configuration ( $I_{\text{lim\_sc}}$ , black-circle and  $D_{\text{app}}$ , orange-triangle, respective) as a function of the various concentrations of  $[\text{Cu}(\text{dmbpy})_2]^{2+}$  from 0.05 M to 0.15 M (the saturation point), and their standard deviations from three different measurements. The red area indicates the physical ionic diffusion dominant region and the red line and curve for  $I_{\text{lim\_sc}}$  and  $D_{\text{app}}$ , respective, are fitted from equation (2) and (3).

The Dahms-Luff equation relates how the apparent diffusion coefficient ( $D_{\text{app}}$ ) is related to the diffusion due to hole-hopping between redox shuttles ( $D_{\text{ex}}$ ) and the physical ionic diffusion ( $D_{\text{phys}}$ ) in liquid solution expressed by equation (1)<sup>16-19</sup>

$$D_{\text{app}} = D_{\text{phys}} + D_{\text{ex}} = D_{\text{phys}} + k_{\text{ex}}\delta^2 c/6 \quad (1)$$

where  $\delta$  is average center-to-center distances between redox shuttles in the encounter complex and  $c$  is the redox shuttle concentration.<sup>16-19</sup> In this work, we use the Dahms-Luff equation to reveal the mechanism trajectories of charge transport from the liquid phase of LE to the solid phase of HTM within copper complexes. Since the diffusion of LEs and HTMs are dominated by ion movements, and the hole-hopping, respectively,<sup>5</sup> they can be understood using different mechanisms. Therefore, an important parameter should be introduced to distinguish the two different mechanisms is the self-exchange charge transfer rate constant ( $k_{\text{ex}}$ ). The  $k_{\text{ex}}$  directly

relates the diffusion in charge transport to the reorganization energy of copper complexes in both the LE and the HTM.<sup>20-24</sup> The  $k_{\text{ex}}$  generally has little influence on the overall diffusion in the LE where the distance between molecules are far from each other, but in the HTM, it can dominate diffusion as described by a hopping mechanism as  $k_{\text{ex}} = K_{\text{a}}k_{\text{hop}}$ , where  $K_{\text{a}}$  is the association constant of the bimolecular rate equation and  $k_{\text{hop}}$  is the hopping frequency in the bimolecular charge transfer.<sup>21, 25-26</sup> Therefore, by tracking the change in the  $D_{\text{app}}$  with the concentration using the Dahms-Luff equation, the dominant diffusion mechanism can be discerned.

From measurements of the mass transport limiting current, the values of  $D_{\text{app}}$  can be calculated for a sandwich cell configuration from (2)<sup>27</sup>

$$I_{\text{lim\_sc}} = FAD_{\text{app}}c/d = FA(D_{\text{phys}} + D_{\text{ex}})c/d = FA(D_{\text{phys}}c + k_{\text{ex}}\delta^2c^2/6)/d \quad (2)$$

where  $I_{\text{lim\_sc}}$  is the diffusion-limited current from the sandwich cell configuration,  $F$  is the Faraday constant,  $A$  is the active area of sandwich configurations,  $d$  is the distance between the two electrodes at the sandwich cell. The above equation indicates that the mass transport limited current is a concentration dependent function, which varies linearly with concentration in the physical ionic diffusion regime and quadratically with concentration in the hole-hopping regime. Thus, plotting  $I_{\text{lim\_sc}}$  values vs concentration allows the ability to distinguish a change of the diffusion from the LE to the HTM.

Measurements of the  $I_{\text{lim\_sc}}$  show it decreases during solvent evaporation, which may be due to a decreasing  $D_{\text{app}}$ , as shown in Figure S5. However, the active area of the electrode/electrolyte interface certainly decreases with time during the solvent evaporation, which may account for the decreasing  $I_{\text{lim\_sc}}$ . In addition, as the solvent evaporates, the concentration of the redox species increases with time which should also affect the  $I_{\text{lim\_sc}}$  independent of changes in diffusion coefficient or mechanism. At a minimum, these considerations impose significant uncertainty in

determination of diffusion.

We subsequently employed a second method to determine the trajectory of diffusion mechanism from the LE to the HTM using the sandwich configuration cell by intentionally varying the  $[\text{Cu}(\text{dmbpy})_2]^{2+/+}$  concentrations in electrolytes. In this case the electroactive surface area is known and constant and variations in  $I_{\text{lim\_sc}}$  can be attributed just to  $D_{\text{app}}$ . The  $I_{\text{lim\_sc}}$  and  $D_{\text{app}}$  measured as a function of  $[\text{Cu}(\text{dmbpy})_2]^{2+/+}$  concentration are plotted in Figure 2b. Although  $[\text{Cu}(\text{dmbpy})_2]^{2+/+}$  exhibits limited solubility in the solvent, the results provide important insights. First, the  $I_{\text{lim\_sc}}$  increases linearly with respect to the concentration of  $[\text{Cu}(\text{dmbpy})_2]^{2+}$  at the low concentration range, as predicted by equation (2). However, unlike the simulation of equation (1) predicting that the  $D_{\text{app}}$  will be constant according to the concentration change in the physical ionic diffusion region, the  $D_{\text{app}}$  is confirmed to decrease rapidly with increasing concentration of  $[\text{Cu}(\text{dmbpy})_2]^{2+}$  (Figure 2b). From this result, it can be deduced that the concentration range of  $[\text{Cu}(\text{dmbpy})_2]^{2+}$  (0 ~ 0.15 M) measured in Figure 2b is in the physical ionic diffusion dominant region. And it also strongly suggests that the  $D_{\text{phys}}$  term of Dahms-Luff equation applied to the above work must be modified.<sup>16-19</sup>

The most likely factor that directly influences the  $D_{\text{phys}}$  parameter is the viscosity ( $\eta$ ) of the solution. The  $\eta$  can be expressed as a function of the solute concentration,  $\eta = \eta_0(1 + Ac + Bc^2 + Dc^3 \dots)$ , where A, B, D, ... are constants and  $\eta_0$  is the initial solvent viscosity.<sup>28</sup> By substituting the above viscosity-concentration equation into Stokes-Einstein equation,  $D_{\text{phys}} = kT/6\pi\eta R_m$ , where  $k$  is the Boltzman constant and  $R_m$  is the solute molecule radius,<sup>29</sup> the relationship between the viscosity of the solution and  $D_{\text{phys}}$ , the polynomial reciprocal function of concentration can be obtained for  $D_{\text{phys}} = kT/6\pi\eta_0(1 + Ac + Bc^2 + Dc^3 \dots)R_m$ . Using this result and equation (1), the modified Dahms-Luff equation is obtained as following equation (3):

$$D_{\text{app}} = D_{\text{phys}} + D_{\text{ex}} = kT/6\pi\eta_0(1 + Ac + Bc^2 + Dc^3 \cdots)R_m + k_{\text{ex}}\delta^2c/6 \quad (3)$$

Equation (3) accurately represents the result for the  $D_{\text{app}}$  by the sandwich configuration measurement in Figure 2b. Thus, in the physical ionic diffusion region where the concentration is relatively low, the value of  $D_{\text{app}}$  decreases rapidly according to the polynomial reciprocal function of the concentration due to increasing viscosity. However, if the concentration still increases, and the system has a high  $k_{\text{ex}}$ , the  $D_{\text{ex}}$  would dominate the overall  $D_{\text{app}}$  as indicated by the right-hand side of equation (3); in this case  $D_{\text{app}}$  would increase linearly with the concentration.

In order to test these predictions, we performed *in-situ* measurements with an UME. This system was developed to directly monitor the diffusion mechanism for the solidifying intermediate state and the HTM of  $[\text{Cu}(\text{dmbpy})_2]^{2+/+}$ . The very small surface area of the UME minimizes the ohmic drop from the contact between the electrode and the solute caused by the solvent evaporation, and maintains a constant contact area.<sup>30-31</sup> The overall experimental set-up is illustrated in Supporting Information, Figure S8. From the calculated solvent evaporation rate, we directly observe the change of  $[\text{Cu}(\text{dmbpy})_2]^{2+}$  concentrations according to the evaporation time of the solvent, and consequently, the monitored results of  $I_{\text{lim}}$  can be obtained directly according to the concentration changes of  $[\text{Cu}(\text{dmbpy})_2]^{2+}$  (see Supporting Information, Figure S9).

Figure 3a shows the  $I_{\text{lim}}$  versus the molar concentration of  $[\text{Cu}(\text{dmbpy})_2]^{2+}$ . Considering the geometry of the UME, the  $I_{\text{lim}}$  can be described by equation (4) with the modified Dahms-Luff equation (equation (3)) as:

$$I_{\text{lim}} = 4FrD_{\text{app}}c = 2FrkTc/3\pi\eta_0(1 + Ac + Bc^2 + Dc^3 \cdots)R_m + 2Frk_{\text{ex}}\delta^2c^2/3 \quad (4)$$

where  $r$  is the radius of disk UME.<sup>27</sup>

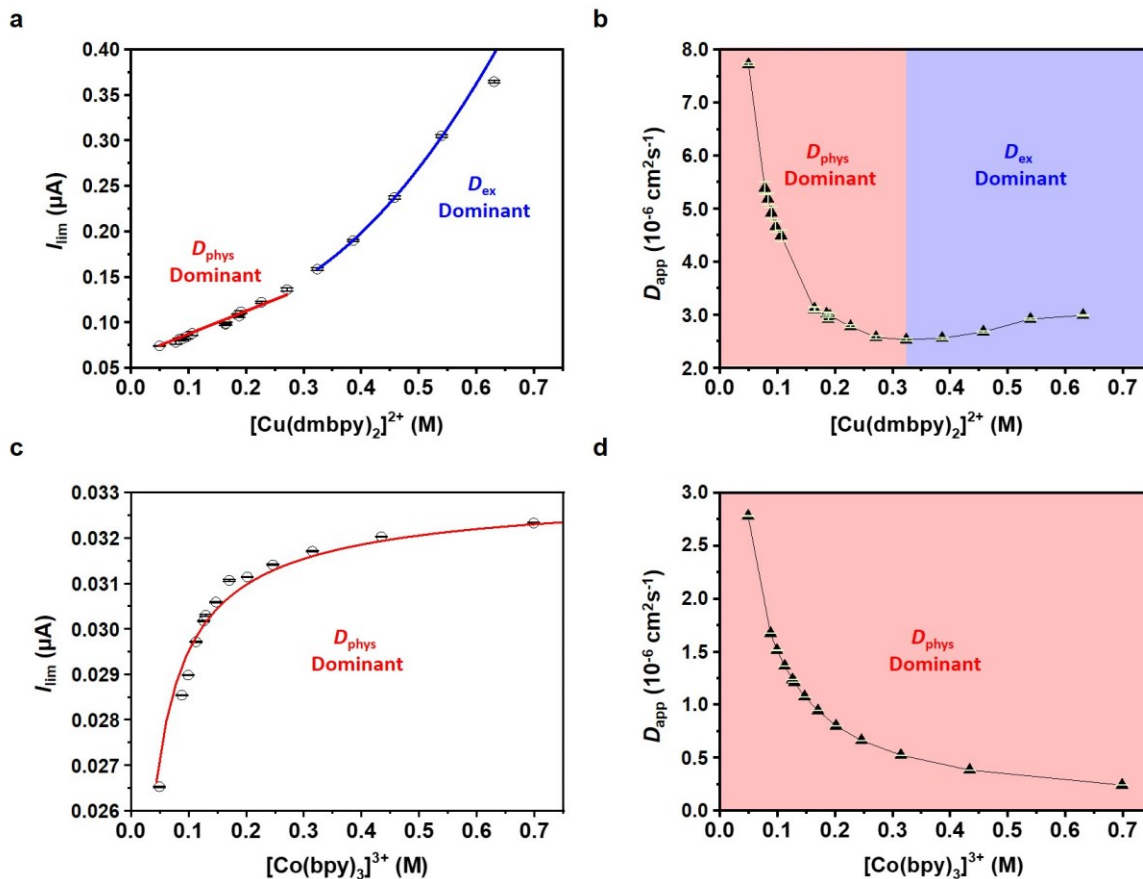


**Figure 3.** (a) Plot of  $I_{lim}$  for the reaction of  $[Cu(dmbpy)_2]^{2+} + e^- \rightarrow [Cu(dmbpy)_2]^+$  as a function of  $[Cu(dmbpy)_2]^{2+}$  concentration. Equation (4) was used to fit the data for the physical ionic diffusion regime ( $D_{phys}$ , red line) and the electronic diffusion regime ( $D_{ex}$ , blue curve). (b) The  $D_{app}$  of  $[Cu(dmbpy)_2]^{2+}$  calculated from equation (3) where the dominant regions for  $D_{phys}$  (red area) and  $D_{ex}$  (blue area) are determined by equation (1). (c) Plot of the  $I_{lim}$  values for the reaction of  $[Co(bpy)_3]^{3+} + e^- \rightarrow [Co(bpy)_3]^{2+}$  as a function of  $[Co(bpy)_3]^{3+}$  concentration. The left term of equation (4) for the  $D_{phys}$  dominant regions was applied to fit the data. (d) The calculated  $D_{app}$  of  $[Co(bpy)_3]^{3+}$  from the results of  $I_{lim}$  as a function of the concentration. The  $D_{phys}$  dominant region was confirmed by equation (3). All data are depicted as mean values and standard deviations.

Interestingly, at low concentration region of  $[Cu(dmbpy)_2]^{2+}$  up to around 0.3 M (Figure 3a), the  $I_{lim}$  increases approximately linearly with respect to the molar concentration of  $[Cu(dmbpy)_2]^{2+}$ , which is consistent with physical ionic diffusion dominating as expected for LEs, in agreement with equation (2). However, as the molar concentration of  $[Cu(dmbpy)_2]^{2+}$  increases over 0.3 M, the  $I_{lim}$  begins to increase by the square of the molar concentration of  $[Cu(dmbpy)_2]^{2+}$  ( $R^2 = 0.999$ ).

These results clearly support that the diffusion mechanism of HTM with  $[\text{Cu}(\text{dmbpy})_2]^{2+/+}$  can be dominated by electronic diffusion, not ionic diffusion, as shown in a previous report.<sup>32</sup>

In the region where electronic diffusion is dominant, the  $k_{\text{ex}}$  in the HTM for the  $[\text{Cu}(\text{dmbpy})_2]^{2+/+}$  can be estimated as  $(8.3 \pm 0.5) \times 10^8 \text{ M}^{-1} \text{ s}^{-1}$  through application of the  $D_{\text{ex}}$  component of equation (4). This rate constant is  $\sim 10^5$  times higher than the  $k_{\text{ex}}$  of the dilute liquid solution ( $8.8 \times 10^3 \text{ M}^{-1} \text{ s}^{-1}$ ) calculated by the NMR line-broadening method (Supporting Information, Figure S11).

The above  $I_{\text{lim}}$  results for the diffusion mechanism change of the  $[\text{Cu}(\text{dmbpy})_2]^{2+/+}$  from the LE to the HTM can also be comprehended in more detail in a trajectory of the  $D_{\text{app}}$  as a function of the molar concentration of  $[\text{Cu}(\text{dmbpy})_2]^{2+}$  (Figure 3b). In accord with the sandwich configuration results (Figure 2b), the  $D_{\text{app}}$  is reduced to the polynomial reciprocal function for the molar concentration of  $[\text{Cu}(\text{dmbpy})_2]^{2+}$  at the low concentration region. However, as the molar concentration of  $[\text{Cu}(\text{dmbpy})_2]^{2+}$  continues to increase, the rate of decrease in the  $D_{\text{app}}$  becomes smaller and eventually when the molar concentration of  $[\text{Cu}(\text{dmbpy})_2]^{2+}$  is 0.352 M, the derivative of the  $D_{\text{app}}$  curve becomes zero. Interestingly, at the high concentration region thereafter, in spite of the  $\eta$  increasing, the  $D_{\text{app}}$  linearly increases. This result agrees well with the prediction through equation (3) for the diffusion of the  $[\text{Cu}(\text{dmbpy})_2]^{2+/+}$ . That is, the overall diffusion mechanism of the  $[\text{Cu}(\text{dmbpy})_2]^{2+/+}$  is dominated by the  $D_{\text{phys}}$  when  $D_{\text{phys}} > D_{\text{ex}}$  at the low concentration region (red region in Figure 3b), and at the high concentration region, as  $D_{\text{phys}} < D_{\text{ex}}$ , the  $D_{\text{ex}}$  dominates the diffusion mechanism (blue region in Figure 3b). Therefore, the complete dried solid of  $[\text{Cu}(\text{dmbpy})_2]^{2+/+}$  has only the pure  $D_{\text{ex}}$  without the  $D_{\text{phys}}$  in the diffusion mechanism for the charge transport.

For comparison,  $[\text{Co}(\text{bpy})_3]^{3+/2+}$  was also investigated as it has a known small  $k_{\text{ex}}$  ( $0.27 \text{ M}^{-1} \text{ s}^{-1}$ )

1).<sup>33</sup> For this complex, only the  $D_{\text{phys}}$  component is needed to describe the transport mechanism represented by both the  $I_{\text{lim}}$  and the  $D_{\text{app}}$  acquired by *in-situ* solidification measurements (Figure 3c and 3d). These results show that even though the redox shuttle distance is getting closer as the solidification progresses, the  $k_{\text{ex}}$  of  $[\text{Co}(\text{bpy})_3]^{3+/2+}$  is too low to support significant  $D_{\text{ex}}$ . This can be attributed to the large inner sphere reorganization energy associated with a high-spin  $[\text{Co}(\text{bpy})_3]^{2+}$  to low-spin  $[\text{Co}(\text{bpy})_3]^{3+}$  electronic change upon charge transfer.<sup>34</sup> With an insignificant contribution of  $D_{\text{ex}}$ , the  $D_{\text{app}}$  continuously reduces due to the increase in  $\eta$ . This result explains why  $[\text{Co}(\text{bpy})_3]^{3+/2+}$  HTMs show very low performance in DSCs unlike the copper complexes which exhibit faster charge transfer self-exchange.<sup>10, 13</sup>

From the  $k_{\text{ex}}$  values determined above, we are in a position to estimate the reorganization energy ( $\lambda$ ) for the copper complexes as a result of the solidification process. This is important because the  $\lambda$  is a factor that affects the interfacial charge transfer (recombination) and dye regeneration reactions in addition to hole transport.<sup>33</sup> Table S1 shows that the calculation results of the  $k_{\text{ex}}$  and the predicted  $\lambda$  for the LE and HTM with  $[\text{Cu}(\text{dmbpy})_2]^{2+/+}$  (Cu-L and Cu-S), and the LE with  $[\text{Co}(\text{bpy})_3]^{3+/2+}$  (Co-L). For  $[\text{Cu}(\text{dmbpy})_2]^{2+/+}$ , the Cu-L  $\lambda$  (1.66 eV) is a result of both inner sphere ( $\lambda_{\text{in}} = 1.00$  eV) and outersphere ( $\lambda_{\text{out}} = 0.66$  eV) components. The solvent (outersphere) reorganization decreases to approximately zero following solidification which decreases the  $\lambda$  accordingly. Interestingly, the  $\lambda_{\text{in}}$  (0.47 eV) also decreases upon phase transition to the HTM (Cu-S). Clearly the  $\lambda_{\text{in}}$  associated with ligand geometry rearrangement generally associated with the change in oxidation state of Cu(I) tetrahedral to Cu(II) square planar complexes is reduced in the solid-state. Thus, the Cu-S appears to decrease even more dramatically from Cu-L than one would presume. The results of this analysis explain how the solidification process reduces the energy barrier of the exchange reaction between copper complexes and increases the charge transfer

reaction rate to produce the higher hole conductivity observed in HTMs compared to LEs. The low  $\lambda$  of the copper complex HTM would be consistent with fast dye regeneration and high quantum yields, as well as fast recombination and sub-optimal photovoltages. A more detailed investigation of the connection between charge transport, dye regeneration, recombination and the overall device performance is in progress in our lab, which will allow development of design rules for HTMs based on metal complexes for photoelectronic applications. The results of this study, however, provide the methodology and the important first milestone in establishing the charge transport mechanism for molecular-based HTMs.

## ASSOCIATED CONTENT

### Supporting Information

Experimental details, electrochemical properties of copper complexes, sandwich configuration results during the *in-situ* solvent evaporation, reproducibility results of the diffusion mechanism trajectory of the  $[\text{Cu}(\text{dmbpy})_2]^{2+/+}$  and  $[\text{Co}(\text{bpy})_3]^{3+/2+}$  from the LE to HTM by the *in-situ* solidifying measurement, NMR line-broadening result for the  $k_{\text{ex}}$  of  $[\text{Cu}(\text{dmbpy})_2]^{2+}$  in LE, crystal structures of  $[\text{Cu}(\text{dmbpy})_2]^{2+/+}$ , calculation of reorganization energies.

## AUTHOR INFORMATION

Corresponding Author

\*E-mail: [hamann@chemistry.msu.edu](mailto:hamann@chemistry.msu.edu).

ORCID

Tea-Yon Kim: 0000-0001-8510-8261

Thomas W. Hamann: 0000-0001-6917-7494

Notes

The authors declare no competing financial interest.

## ACKNOWLEDGMENT

This work was supported by the Chemical Sciences, Geosciences, and Biosciences Division, Office of Basic Energy Sciences, Office of Science, the U.S. Department of Energy Grant No. DE-SC0017342.

## REFERENCE

1. Coropceanu, V.; Cornil, J.; da Silva, D. A.; Olivier, Y.; Silbey, R.; Bredas, J. L. Charge Transport in Organic Semiconductors. *Chem. Rev.* **2007**, *107*, 2165–2165.
2. Hagfeldt, A.; Boschloo, G.; Sun, L.; Kloo, L.; Pettersson, H. Dye-Sensitized Solar Cells. *Chem. Rev.* **2010**, *110*, 6595–6663.
3. Green, M. A.; Ho-Baillie, A.; Snaith, H. J. The Emergence of Perovskite Solar Cells. *Nat. Photon.* **2014**, *8*, 506–514.
4. Docampo, P.; Guldin, S.; Leijtens, T.; Noel, N. K.; Steiner, U.; Snaith, H. J. Lessons Learned: From Dye-Sensitized Solar Cells to All-Solid-State Hybrid Devices. *Adv. Mater.* **2014**, *26*, 4013–4030.
5. Wu, J.; Lan, Z.; Lin, J.; Huang, M.; Huang, Y.; Fan, L.; Luo, G. Electrolytes in Dye-Sensitized Solar Cells. *Chem. Rev.* **2015**, *115*, 2136–2173.
6. Kakiage, K.; Aoyama, Y.; Yano, T.; Oya, K.; Fujisawa, J.; Hanaya, M. Highly-Efficient Dye-

Sensitized Solar Cells with Collaborative Sensitization by Silyl-Anchor and Carboxy-Anchor Dyes. *Chem. Commun.* **2015**, *51*, 15894–15897.

7. Kim, T.-Y.; Wei, W.; Cho, W.; Lee, S.; Won, J.; Kang, Y. S. Excellent Optical and Interfacial Performance of a PEDOT-*b*-PEG Block Copolymer Counter Electrode for Polymer Electrolyte-Based Solid-State Dye-Sensitized Solar Cells. *Chem. Commun.* **2015**, *51*, 16782–16785.

8. Cao, Y.; Saygili, Y.; Ummadisingu, A.; Teuscher, J.; Luo, J.; Pellet, N.; Giordano, F.; Zakeeruddin, S. M.; Moser, J. E.; Freitag, M.; Hagfeldt, A.; Grätzel, M. 11% Efficiency Solid-State Dye-Sensitized Solar Cells with Copper(II/I) Hole Transport Materials. *Nat. Commun.* **2017**, *8*, 15390.

9. Freitag, M.; Daniel, Q.; Pazoki, M.; Sveinbjornsson, K.; Zhang, J.; Sun, L.; Hagfeldt, A.; Boschloo, G. High-Efficiency Dye-Sensitized Solar Cells with Molecular Copper Phenanthroline as Solid Hole Conductor. *Energy Environ. Sci.* **2015**, *8*, 2634–2637.

10. Cao, Y.; Liu, Y.; Zakeeruddin, S. M.; Hagfeldt, A.; Grätzel, M. Direct Contact of Selective Charge Extraction Layers Enables High-Efficiency Molecular Photovoltaics. *Joule* **2018**, *2*, 1108–1117.

11. Zhang, W.; Wu, Y.; Bahng, H. W.; Cao, Y.; Yi, C.; Saygili, Y.; Luo, J.; Liu, Y.; Kavan, L.; Moser, J. E.; Hagfeldt, A.; Tian, H.; Zakeeruddin, S. M.; Zhu, W.-H.; Grätzel, M. Comprehensive Control of Voltage Loss Enables 11.7% Efficient Solid-State Dye-Sensitized Solar Cells. *Energy Environ. Sci.* **2018**, *11*, 1779–1787.

12. Kavan, L.; Saygili, Y.; Freitag, M.; Zakeeruddin, S. M.; Hagfeldt, A.; Grätzel, M. Electrochemical Properties of Cu(II/I)-Based Redox Mediators for Dye-Sensitized Solar Cells. *Electrochim. Acta* **2017**, *227*, 194–202.

13. Kashif, M. K.; Milhuisen, R. A.; Nippe, M.; Hellerstedt, J.; Zee, D. Z.; Duffy, N. W.; Halstead, B.; De Angelis, F.; Fantacci, S.; Fuhrer, M. S.; Chang, C. J.; Cheng, Y.-B.; Long, J. R.; Spiccia, L.; Bach, U. Cobalt Polypyridyl Complexes as Transparent Solution-Processable Solid-State Charge Transport Materials. *Adv. Energy Mater.* **2016**, *6*, 1600874.

14. Kashif, M. K.; Benesperi, I.; Milhuisen, R. A.; Meyer, S.; Hellerstedt, J.; Zee, D.; Duffy, N. W.; Halstead, B.; Fuhrer, M. S.; Cashion, J.; Cheng, Y.-B.; Spiccia, L.; Simonov, A. N.; Bach, U. Polypyridyl

Iron Complex as a Hole-Transporting Material for Formamidinium Lead Bromide Perovskite Solar Cells. *ACS Energy Letters* **2017**, *2*, 1855–1859.

15. Wang, P.; Zakeeruddin, S. M.; Moser, J. E.; Nazeeruddin, M. K.; Sekiguchi, T.; Grätzel, M. A Stable Quasi-Solid-State Dye-Sensitized Solar Cell with an Amphiphilic Ruthenium Sensitizer and Polymer Gel Electrolyte. *Nat. Mater.* **2003**, *2*, 498–498.

16. Blauch, D. N.; Saveant, J.-M. Dynamics of Electron Hopping in Assemblies of Redox Centers - Percolation and Diffusion. *J. Am. Chem. Soc.* **1992**, *114*, 3323–3332.

17. Dahms, H. Electronic Conduction in Aqueous Solution. *J. Phys. Chem.* **1968**, *72*, 362–364.

18. Ruff, I.; Friedrich, V. J. Transfer diffusion. I. Theoretical. *J. Phys. Chem.* **1971**, *75*, 3297–3302.

19. Buttry, D. A.; Anson, F. C. Electron Hopping vs. Molecular-Diffusion as Charge-Transfer Mechanisms in Redox Polymer-Films. *J. Electroanal. Chem.* **1981**, *130*, 333–338.

20. Marcus, R. A.; Sutin, N. Electron Transfers in Chemistry and Biology. *Biochim. Biophys. Acta* **1985**, *811*, 265–322.

21. Sutin, N. Theory of Electron-Transfer Reactions - Insights and Hintsights. *Prog. Inorg. Chem.* **1983**, *30*, 441–498.

22. Hamann, T. W.; Gstrein, F.; Brunschwig, B. S.; Lewis, N. S. Measurement of the Dependence of Interfacial Charge-Transfer Rate Constants on the Reorganization Energy of Redox Species at n-ZnO/H<sub>2</sub>O Interfaces. *J. Am. Chem. Soc.* **2005**, *127*, 13949–13954.

23. Surridge, N. A.; Jernigan, J. C.; Dalton, E. F.; Buck, R. P.; Watanabe, M.; Zhang, H.; Pinkerton, M.; Wooster, T. T.; Longmire, M. L.; Facci, J. S.; Murray, R. W. Electron Self-Exchange Dynamics between Redox Sites in Polymers. *Faraday Discuss. Chem. Soc.* **1989**, *88*, 1–17.

24. Lin, S.; Usov, P. M.; Morris, A. J. The Role of Redox Hopping in Metal-Organic Framework Electrocatalysis. *Chem. Commun.* **2018**, *54*, 6965–6974.

25. Grampp, G.; Rasmussen, K. Solvent Dynamical Effects on the Electron Self-Exchange Rate of the TEMPO/TEMPO<sup>+</sup> Couple (TEMPO=2,2,6,6-tetramethyl-1-piperidinyloxy radical) - Part 1. ESR-Linebroadening Measurements at T=298 K. *Phys. Chem. Chem. Phys.* **2002**, *4*, 5546–5549.

26. Sato, K.; Ichinoi, R.; Mizukami, R.; Serikawa, T.; Sasaki, Y.; Lutkenhaus, J.; Nishide, H.; Oyaizu, K. Diffusion-Cooperative Model for Charge Transport by Redox-Active Nonconjugated Polymers. *J. Am. Chem. Soc.* **2018**, *140*, 1049–1056.
27. Rutkowska, I. A.; Marszalek, M.; Orłowska, J.; Ozimek, W.; Zakeeruddin, S. M.; Kulesza, P. J.; Gratzel, M. Nanocomposite Semi-Solid Redox Ionic Liquid Electrolytes with Enhanced Charge-Transport Capabilities for Dye-Sensitized Solar Cells. *Chemsuschem* **2015**, *8*, 2560–2568.
28. Simha, R. Effect of Concentration on the Viscosity of Dilute Solutions. *J. Res. Nat. Bur. Stand.* **1949**, *42*, 409–418.
29. Edward, J. Molecular Volumes and the Stokes-Einstein Equation. *J. Chem. Educ.* **1970**, *47*, 261–270.
30. Wightman, R. M. Voltammetry with Microscopic Electrodes in New Domains. *Science* **1988**, *240*, 415–420.
31. Heinze, J. Ultramicroelectrodes in Electrochemistry. *Angew. Chem. Int. Ed.* **1993**, *32*, 1268–1288.
32. Kawano, R.; Watanabe, M. Equilibrium Potentials and Charge Transport of an I/I<sub>3</sub><sup>-</sup> Redox Couple in an Ionic Liquid. *Chem. Commun.* **2003**, 330–331.
33. Xie, Y. L.; Baillargeon, J.; Hamann, T. W. Kinetics of Regeneration and Recombination Reactions in Dye-Sensitized Solar Cells Employing Cobalt Redox Shuttles. *J. Phys. Chem. C* **2015**, *119*, 28155–28166.
34. Xie, Y. L.; Hamann, T. W. Fast Low-Spin Cobalt Complex Redox Shuttles for Dye-Sensitized Solar Cells. *J. Phys. Chem. Lett.* **2013**, *4*, 328–332.